

Vacuum energy decay from a q-bubble

F.R. Klinkhamer*

*Institute for Theoretical Physics,
Karlsruhe Institute of Technology (KIT), 76128 Karlsruhe, Germany*

O.P. Santillán†

*Departamento de Matemáticas Luis Santaló (IMAS),
UBA CONICET, Buenos Aires, Argentina*

G.E. Volovik‡

*Low Temperature Laboratory, Department of Applied Physics,
Aalto University, PO Box 15100, FI-00076 Aalto, Finland,
and*

*Landau Institute for Theoretical Physics, Russian Academy of Sciences,
Kosyginaya 2, 119334 Moscow, Russia*

A. Zhou§

*Institute for Theoretical Physics,
Karlsruhe Institute of Technology (KIT), 76128 Karlsruhe, Germany*

Abstract

We consider a finite-size spherical bubble with a nonequilibrium value of the q -field, where the bubble is immersed in an infinite vacuum with the constant equilibrium value q_0 for the q -field. Numerical results are presented for the time evolution of such a q -bubble with gravity turned off ($G_N = 0$) and with gravity turned on ($G_N > 0$ and ratio of energy scales $E_{q\text{-field}}/E_{\text{Planck}} \sim 1/10$). For small enough bubbles and energy scale $E_{q\text{-field}}$ sufficiently below the gravitational energy scale E_{Planck} , the vacuum energy of the q -bubble is found to disperse completely. For large enough bubbles and nonzero G_N , the vacuum energy of the q -bubble disperses only partially and gravitational collapse occurs near the bubble center.

PACS numbers: 95.36.+x, 98.80.Es, 98.80.Jk

Keywords: dark energy, cosmological constant, cosmology

* frans.klinkhamer@kit.edu

† osantil@dm.uba.ar

‡ volovik@ltl.tkk.fi

§ albert.zhou@kit.edu

I. INTRODUCTION

The energy density of the vacuum, the dark energy, and the cosmological constant are highly debated topics today, as quantum field theory suggests a typical number that is some 120 orders of magnitude larger [1, 2] than what has been observed [3]. The mismatch is so large and so significant as to make it the main outstanding problem of modern physics. However, a similar vacuum energy problem exists in condensed matter systems, and its solution may provide a hint for the solution of the cosmological constant puzzle. In condensed matter, the zero-point energy of the quantum fields is fully cancelled by the microscopic (atomic) degrees of freedom, if the system is in its ground state. If the system is slightly out of equilibrium, the vacuum energy is not fully compensated, but its magnitude is determined by the infrared energy scale rather than by the ultraviolet (atomic) energy scale.

Still, in order to apply this condensed matter scenario of the cancellation of the vacuum energy to the quantum vacuum of our Universe, we need to know the proper variable to describe the deep quantum vacuum. One example of such a variable is the four-form field strength used by Hawking, in particular [4]. The nonlinear extension of this approach, which goes under the name of q -theory [5, 6], demonstrates the nullification of the vacuum energy density in a full-equilibrium vacuum without matter present. A small cosmological constant appears if the vacuum is out of equilibrium. Its value is then determined by infrared physics and is proportional either to the matter content of the Universe or to the expansion rate.

While q -theory solves the main cosmological problem (other realizations of the q variable are presented in Refs. [7, 8]), the dynamical process of equilibration of the vacuum towards the full equilibrium is still under the investigation. The previously obtained results [6] concern the decay of an initially homogeneous high-energy state emerging immediately after the Big Bang. These calculations demonstrated that, with generic initial conditions, the high-energy state prefers to relax to a de-Sitter vacuum rather than to the Minkowski vacuum. On the other hand, the possibility of the final decay of the de-Sitter vacuum to the Minkowski vacuum is under intensive debate. This is because of the special symmetry of de-Sitter spacetime; see, e.g., Refs. [9, 10] and references therein.

One way to circumvent this de-Sitter controversy is to consider the case that the Big Bang takes place not over the whole of space but only in a finite region of space, which is surrounded by equilibrium Minkowski vacuum. This possibility is also suggested by condensed matter experiments [11], where the hot spot created within the equilibrium state finally relaxes to the full equilibrium by radiating the extra energy away to infinity.

Concretely, we propose to calculate, in the q -theory framework [5, 6], the time evolution of a finite-size spherical bubble with $q \neq q_0$, which is immersed in an infinite equilibrium vacuum with $q = q_0$. The expectation is that the interior field $q(r, t)$ relaxes to q_0 , while the bubble wall (or its remnant) ultimately moves outwards. Yet, gravity may hold surprises in store. Remark that our proposed calculation corresponds to the scenario discussed in the second paragraph of Sec. V A in Ref. [6], which mentioned the possibility that “the starting nonequilibrium state could, in turn, be obtained by a large perturbation of an

initial equilibrium vacuum.”

Before we start with this calculation, we have two clarifying comments. The first comment is that it may be instructive to compare our q -bubble to the vacuum bubble as discussed by Coleman and collaborators [12–14]. That discussion starts from a classical field theory of a fundamental scalar field ϕ with nonderivative interactions. The interactions are, in fact, determined by a potential term $V(\phi)$ in the action. The potential $V(\phi)$ is assumed to have various local minima: one or more “false” vacua $\phi_{+,n}$ and the single “true” vacuum ϕ_- , where the “false” vacua have a larger energy density $V(\phi_{+,n})$ than the value $V(\phi_-)$ of the “true” vacuum. Coleman’s vacuum bubble, then, corresponds to a finite-size spherical bubble with “true” vacuum inside and “false” vacuum outside (in other words, the energy density inside is lower than outside). The dynamic behavior of a single vacuum bubble is that the bubble expands (cf. Fig. 4 in Ref. [12]) with the true-vacuum region increasing but, at a given finite time, the far-away region remaining in a false-vacuum state. Such a vacuum bubble is essentially different from our q -bubble which has an infinite equilibrium vacuum with $q = q_0$ outside (in Coleman’s terminology, “true” q -vacuum outside). In a way, the q -bubble resembles Coleman’s vacuum bubble with interior and exterior regions switched. It is clear that, already energetically, the dynamic behavior of the q -bubble will be different from that of Coleman’s vacuum bubble.

The second comment concerns the different role of a fundamental scalar field ϕ and the vacuum variable q for the cosmological constant problem. In the fundamental-scalar-field approach, the nullification of the energy density $\rho_V(\phi) = \epsilon(\phi)$ in the equilibrium vacuum requires fine-tuning [2]. In the q -field approach, the vacuum is a self-sustained system, which, in equilibrium, automatically acquires a zero value for the thermodynamic potential $\rho_V(q) = \epsilon(q) - q d\epsilon(q)/dq$ that enters the Einstein equation by a cosmological-constant-type term. See, in particular, the discussion of Sec. 2 in Ref. [7].

We, now, turn to the calculation of the time evolution of a q -bubble. After a brief discussion of the theory, we, first, consider a q -bubble with gravity effects turned off and, then, with gravity effects turned on. Throughout, we use natural units with $c = \hbar = 1$ and take the metric signature $(- +++)$.

II. THEORY AND SETUP

In this article, we will use q -theory in the four-form-field-strength realization with explicit derivative terms of the q -field in the action [15–18]. Specifically, we take the simplest possible theory with the following action [17]:

$$S = - \int_{\mathbb{R}^4} d^4x \sqrt{-g} \left(\frac{R}{16\pi G_N} + \epsilon(q) + \frac{1}{2} (q_0)^{-1} g^{\alpha\beta} (\nabla_\alpha q) (\nabla_\beta q) \right), \quad (2.1a)$$

$$F_{\alpha\beta\gamma\delta} \equiv \nabla_{[\alpha} A_{\beta\gamma\delta]}, \quad (2.1b)$$

$$F_{\alpha\beta\gamma\delta} = q \sqrt{-g} \epsilon_{\alpha\beta\gamma\delta}, \quad (2.1c)$$

where A is a three-form gauge field with a corresponding four-form field strength $F \propto q$ (see Refs. [5, 6] and further references therein) and $\epsilon(q)$ is a generic even function of q . We use the same conventions for the curvature tensors as in Ref. [19]. For the moment, we have omitted in the integrand on the right-hand side of (2.1a) the Lagrange density of the fields of the Standard Model of elementary particle physics.

The Hamilton principle for variations $\delta A_{\alpha\beta\gamma}$ and $\delta g_{\mu\nu}$ of the action (2.1) produces two field equations, a generalized Maxwell equation involving $d\epsilon(q)/dq$ and the Einstein equation involving $\rho_V(q) \equiv \epsilon(q) - q d\epsilon(q)/dq$. These two equations are given by (3) and (5), respectively, in Ref. [16]. One particular solution has the flat-spacetime Minkowski metric $g_{\mu\nu}(x) = \eta_{\mu\nu}$ and the constant q -field $q(x) = q_0$, where $q_0 > 0$ corresponds to the equilibrium value of the q -field with $\rho_V(q_0) = -P_V(q_0) = 0$. Note that the mass dimension of q_0 is 2 in the four-form-field-strength realization.

Using q_0 , we introduce the dimensionless coordinates (τ, ρ) for (r, t) , the dimensionless function $f(\tau, \rho)$ for $q(r, t)$, the dimensionless constant u_0 for μ_0 , and the dimensionless vacuum energy density $r_V(f)$ for $\rho_V(q)$. Recall that μ_0 is the equilibrium value of the “chemical potential” $\mu(q)$ corresponding to the conserved vacuum variable q ; see Ref. [5] for further discussion.

In order to be specific, we take the following *Ansatz* for the dimensionless energy density $\epsilon(f)$ appearing in the action (2.1a):

$$\epsilon(f) = h \left[\frac{1}{2} (f^4/3 - f^2) + \frac{1}{16} (1 - f)^4 \right], \quad (2.2)$$

with a dimensionless prefactor $h > 0$, which, for now, is set to one. The dimensionless gravitating vacuum energy density $r_V(f)$ is given by

$$r_V(f) = \epsilon(f) - u_0 f, \quad (2.3a)$$

$$u_0 = -h/3, \quad (2.3b)$$

where the numerical value from (2.3b) holds for the specific *Ansatz* (2.2).

There are two minima of $r_V(f)$,

$$f = f_0 = 1, \quad (2.4a)$$

$$f = \bar{f} = -(1 + 2\sqrt{3})/11 \approx -0.41, \quad (2.4b)$$

with

$$r_V(f_0) = 0, \quad (2.5a)$$

$$(\chi_0)^{-1} \equiv \left[f^2 \frac{d^2 \epsilon}{df df} \right]_{f=f_0} = h > 0, \quad (2.5b)$$

$$r_V(\bar{f}) \approx +0.03 h, \quad (2.5c)$$

where χ_0 in (2.5b) is the dimensionless version of the equilibrium vacuum compressibility [5].

III. BUBBLE WITHOUT GRAVITY

A. Preliminaries

It is relatively easy to get a result for a special case. First, we set

$$G_N = 0, \quad (3.1)$$

so that we just have Minkowski spacetime to consider. In addition, we set $h = 1$ in (2.2) and (2.3).

Second, we note that the generalized Maxwell equation [5, 6] gives rise to the nonlinear-Klein–Gordon equation (2.4) from Ref. [17], which reads explicitly

$$\square q = q_0 \frac{d\rho_V}{dq}, \quad (3.2)$$

with the flat-spacetime d'Alembertian $\square \equiv \eta^{\alpha\beta} \partial_\alpha \partial_\beta = -\partial_t^2 + \nabla^2$.

Third, introducing spherical coordinates, the q -field of a spherical bubble is given by

$$q = q(t, r). \quad (3.3)$$

Fourth, we start from a bubble with essentially $q_{\text{inside}} = \bar{q} \neq q_0$ and $q_{\text{outside}} = q_0$. The question, then, is how such an q -field configuration evolves with time.

B. Numerics

The numerical solution will be obtained by use of the dimensionless variables introduced in Sec. II. The partial differential equation (PDE) from (3.2) for the spherically symmetric q -field (3.3) then reads

$$\partial_\tau^2 f(\tau, \rho) - \frac{1}{\rho^2} \partial_\rho [\rho^2 \partial_\rho f(\tau, \rho)] = - \left[\frac{d}{df} r_V(f) \right]_{f=f(\tau, \rho)}, \quad (3.4)$$

where $r_V(f)$ is given by (2.2) and (2.3). The initial values and boundary conditions are

$$f(0, \rho) = f_{\text{start}}(\rho), \quad (3.5a)$$

$$\partial_\tau f(0, \rho) = 0, \quad (3.5b)$$

$$\partial_\rho f(\tau, 0) = 0, \quad (3.5c)$$

$$f(\tau, \infty) = f_0. \quad (3.5d)$$

Practically, we restrict the ρ range to $\{\rho_{\min}, \rho_{\max}\}$ with $\rho_{\min} \geq 0$ and $\rho_{\max} < \infty$. Also, we use the following explicit start function:

$$f_{\text{start}}(\rho) = \begin{cases} \bar{f}, & \text{for } \rho \in (0, \bar{\rho} - 1/2), \\ \bar{f} + \sin^2 \left[(\rho - \bar{\rho} + 1/2) \pi/2 \right] (f_0 - \bar{f}), & \text{for } \rho \in [\bar{\rho} - 1/2, \bar{\rho} + 1/2], \\ f_0, & \text{for } \rho \in (\bar{\rho} + 1/2, \infty), \end{cases} \quad (3.6)$$

where, for now, we set $\bar{\rho} = 1$.

The general behavior of the numerical solution is shown in Fig. 1 and time-slices are given in Fig. 2. These results show the disappearance of the bubble “domain-wall” and the start of the outward motion of its remnant. Observe, in Fig. 1, both spatial r_V oscillations (for example, at $\tau = 2$) and temporal r_V oscillations (for example, at $\rho = 0$). The temporal r_V oscillations were first observed for a homogeneous context in Ref. [6], but new here is that energy can escape towards the surrounding unperturbed space.

Other numerical results focus on the out-moving r_V disturbance, triggered by a small initial bubble with $\rho \lesssim 2$. Here, the start function is

$$\tilde{f}_{\text{start}}(\rho) = \bar{f} + \left[1 - \exp(-\rho^2)\right] (f_0 - \bar{f}). \quad (3.7)$$

The numerical solution is shown in Fig. 3 as a surface plot and in Fig. 4 with time slices. These results demonstrate that the out-moving r_V disturbance has a rapidly decreasing amplitude. Incidentally, the quality of the numerical solution can be monitored by evaluating the numerical value of the integral of motion (energy) corresponding to the field equation (3.4); see also Sec. IV B.

C. Discussion

The numerical results of Sec. III B show two characteristics of the q -bubble time evolution in the absence of gravitational effects:

1. initially, the bubble wall gives rise to both out-moving and in-moving ρ_V disturbances, where the in-moving disturbance makes for an increased energy density at the center;
2. ultimately, there is an out-moving ρ_V disturbance with a rapidly diminishing amplitude.

Even for the simple case of zero gravity, this makes the numerical calculation of large bubbles difficult: there are, then, two very different scales, namely the bubble radius ($\bar{\rho} \gg 1$) and the width of the bubble wall ($\Delta\rho \sim 1$).

Remark, finally, that the above two characteristics of the q -bubble dynamics are very different from those of Coleman’s vacuum bubble, as mentioned already in Sec. I. Indeed, Coleman’s vacuum bubble [12] has no in-moving disturbance and an essentially constant domain-wall profile in its rest-frame, energy being supplied by the “false” vacuum.

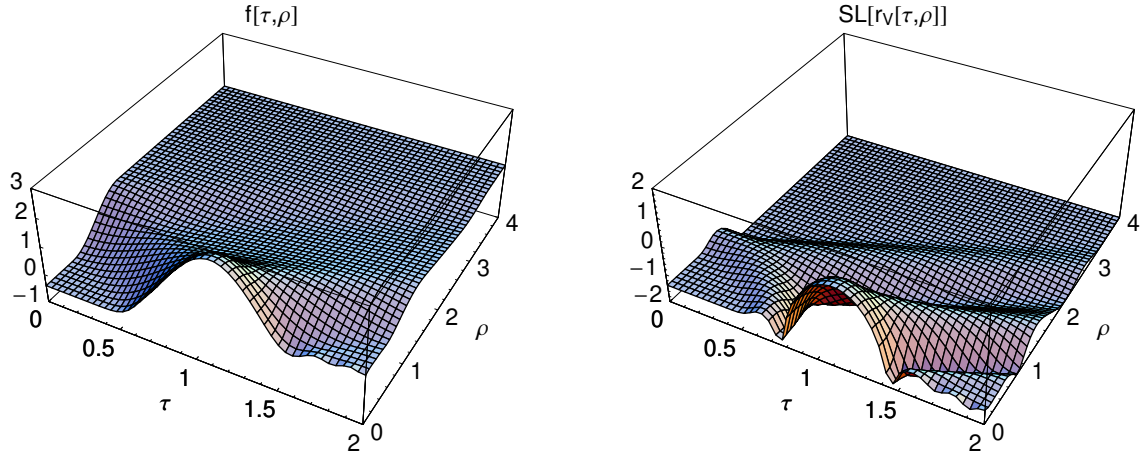


FIG. 1. Numerical solution of the flat-spacetime PDE (3.4) with initial values (3.5a) for the start function (3.6) with $\bar{\rho} = 1$ and (3.5b) and boundary conditions (3.5c) at $\rho_{\min} = 0$ and (3.5d) at $\rho_{\max} = 4$. The $f(\tau, \rho)$ field is calculated over a relatively short time interval, $\tau \in [0, 2]$. Also plotted is the corresponding energy density r_V , using the shift-log function defined by $SL(x) \equiv \log_{10}(x + 0.01) \in [-2, \infty)$ for $x \geq 0$. This vacuum energy density $r_V[f]$ is given by (2.2) and (2.3), with $h = 1$. The vacuum energy density $r_V[f]$ is, in fact, the quantity that would gravitate if G_N were nonzero.

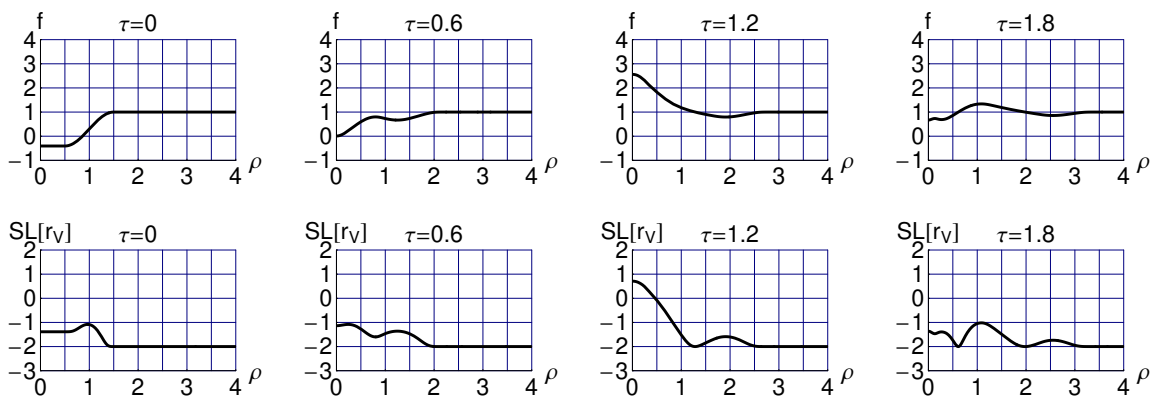


FIG. 2. Four time-slices from the numerical solution of Fig. 1.

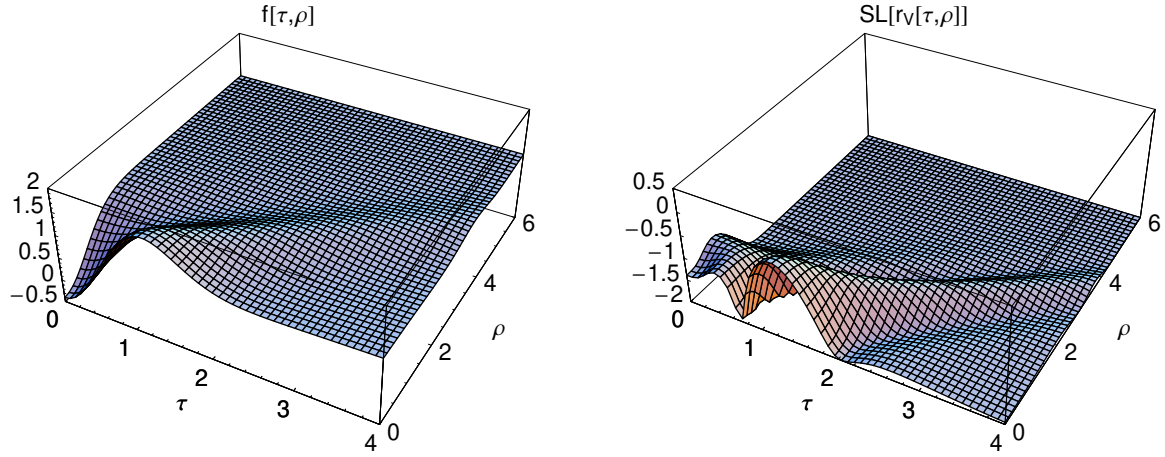


FIG. 3. Same as Fig. 1, but with initial value $f(0, \rho) = \tilde{f}_{\text{start}}(\rho)$ for the start function (3.7).

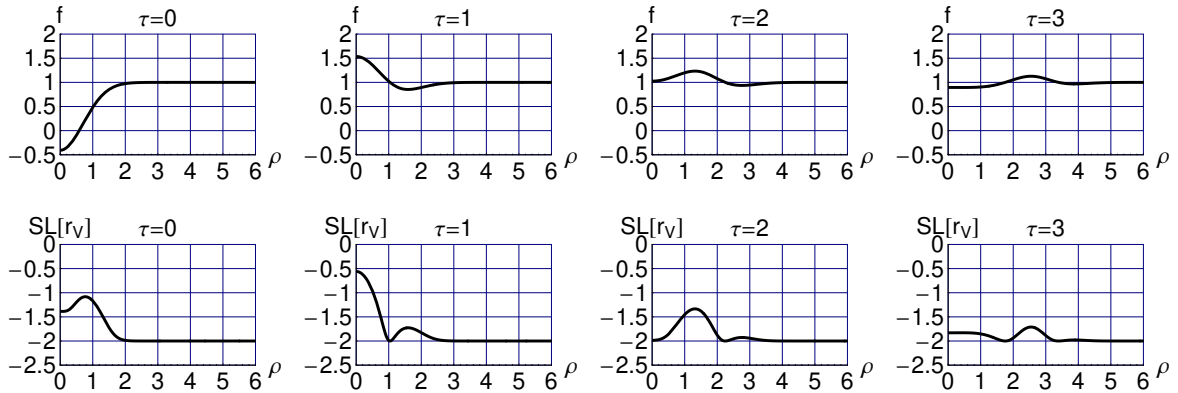


FIG. 4. Four time-slices from the numerical solution of Fig. 3.

IV. BUBBLE WITH GRAVITY

A. Ansätze

The spherically symmetric *Ansatz* for the metric in Kodama–Schwarzschild coordinates (t, r, θ, ϕ) reads [20]

$$g_{\alpha\beta} = \text{diag} \left(-e^{-2\Phi(t, r)} \left[1 - \frac{2G_N m(t, r)}{r} \right], \left[1 - \frac{2G_N m(t, r)}{r} \right]^{-1}, r^2, r^2 \sin^2 \theta \right), \quad (4.1)$$

and the spherically symmetric *Ansatz* for the matter field is simply

$$q = q(t, r). \quad (4.2)$$

It is a straightforward exercise to insert these *Ansätze* into the field equations [16, 17] from the action (2.1). In this way, the reduced nonlinear-Klein–Gordon equation and the reduced Einstein equations are obtained (these expressions will be given in Sec. IV B).

B. Dimensionless PDEs

As mentioned in Sec. II, we make all variables dimensionless by use of $q_0 > 0$, which we now take to have the following numerical value:

$$q_0 = g(G_N)^{-1} \equiv g(E_{\text{Planck}})^2 \approx g (1.22 \times 10^{19} \text{ GeV})^2, \quad (4.3)$$

so that $G_N = g/q_0 \rightarrow 0$ for $g \rightarrow 0^+$ at fixed q_0 . With $q_0 \equiv (E_{q\text{-field}})^2$, the number $g \geq 0$ can be interpreted as a hierarchy factor,

$$g = (E_{q\text{-field}}/E_{\text{Planck}})^2. \quad (4.4)$$

Added to our previous dimensionless q -field *Ansatz* function $f(\tau, \rho)$, we now have two dimensionless metric *Ansatz* functions, making for a total of three *Ansatz* functions:

$$\left\{ f(\tau, \rho), \Phi(\tau, \rho), \mu(\tau, \rho) \right\}. \quad (4.5)$$

A useful definition is

$$B(\tau, \rho) \equiv 1 - 2\mu(\tau, \rho)/\rho, \quad (4.6)$$

as precisely this combination enters the metric *Ansatz* (4.1).

The reduced nonlinear-Klein–Gordon equation then reads

$$\frac{e^{2\Phi}}{B} \ddot{f} - B \frac{1}{\rho^2} \partial_\rho \left(\rho^2 f' \right) + \frac{e^{2\Phi}}{B} \left(\dot{\Phi} + \frac{2\dot{\mu}}{\rho B} \right) \dot{f} + \left(B \Phi' + \frac{2\mu'}{\rho} - \frac{2\mu}{\rho^2} \right) f' = -\frac{dr_V}{df}, \quad (4.7)$$

where an overdot stands for differentiation with respect to τ and a prime for differentiation with respect to ρ . The reduced Einstein equations give the following first-order equations:

$$\frac{\mu'}{\rho^2} = 4\pi g \left[r_V + B \frac{1}{2} (f')^2 + \frac{e^{2\Phi}}{B} \frac{1}{2} (\dot{f})^2 \right], \quad (4.8a)$$

$$\frac{\dot{\mu}}{\rho^2 B} = 4\pi g f' \dot{f}, \quad (4.8b)$$

$$\frac{\Phi'}{\rho} B = 8\pi g r_V - 2\mu'/\rho^2, \quad (4.8c)$$

and the following second-order equation:

$$\frac{\mu''}{\rho} + \frac{e^\Phi}{\rho \sqrt{B}} \partial_\rho \left[\rho B^{3/2} e^{-\Phi} \Phi' \right] + \frac{e^\Phi}{\rho} \partial_\tau \left[\frac{e^\Phi}{B^2} \dot{\mu} \right] = 8\pi g \left\{ r_V + B \frac{1}{2} (f')^2 - \frac{e^{2\Phi}}{B} \frac{1}{2} (\dot{f})^2 \right\}. \quad (4.9)$$

Note that we have used (4.8a) to get the expression on the right-hand side of (4.8c).

The following consistency check holds: the second-order PDE (4.9) is solved by the solutions of the first-order PDEs (4.8) and the second-order PDE (4.7). It is a well-known fact that the same holds for the reduced ordinary differential equations (ODEs) of the Friedmann–Robertson–Walker universe. Specifically, the second-order reduced Einstein ODE follows from the first-order reduced Einstein ODE (a.k.a. the Friedmann equation) by use of the energy-momentum-conservation relations of the perfect fluid considered. Ultimately, this redundancy of the reduced field equations traces back to the invariance of the theory under general coordinate transformations; cf. Sec. 15.1, p. 473 of Ref. [19].

We, now, obtain a g -independent relation from (4.8a) and (4.8b) in three steps. First, we extract μ' from (4.8a) and take the τ derivative. Second, we extract $\dot{\mu}$ from (4.8b) and take the ρ derivative. Third, we equate the two expressions for $\dot{\mu}'$. The obtained relation is

$$\partial_\tau \left(\rho^2 \left[r_V + B \frac{1}{2} (f')^2 + \frac{e^{2\Phi}}{B} \frac{1}{2} (\dot{f})^2 \right] \right) = \partial_\rho \left(\rho^2 B f' \dot{f} \right), \quad (4.10)$$

which can be interpreted as a current-conservation relation. Indeed, for the setup of our initial-value problem (with $f = f_0 = \text{constant}$ for $\rho \geq \bar{\rho} + 1/2$ at $\tau = 0$), the integral of (4.10) gives the following conserved energy E :

$$E = \sqrt{q_0} \int_0^\infty d\rho 4\pi \rho^2 e, \quad (4.11a)$$

$$e = r_V + B \frac{1}{2} (f')^2 + \frac{e^{2\Phi}}{B} \frac{1}{2} (\dot{f})^2, \quad (4.11b)$$

where the equilibrium value q_0 of the q variable in the four-form-field-strength realization (2.1c) has been used to make lengths and times dimensionless (Sec. II).

Consistent with the expected de-Sitter behavior $m(t, r) \sim r^3$ near the center and the expected Schwarzschild behavior $m(t, r) \sim \text{constant}$ towards spatial infinity, we take the

following boundary conditions on the dimensionless metric function $\mu(\tau, \rho)$:

$$\mu(\tau, 0) = 0, \quad (4.12a)$$

$$\partial_\rho \mu(\tau, \infty) = 0. \quad (4.12b)$$

For the other metric function $\Phi(\tau, \rho)$, we take

$$\Phi(\tau, 0) = 0, \quad (4.12c)$$

$$\partial_\rho \Phi(\tau, \infty) = 0. \quad (4.12d)$$

The boundary conditions on $f(\tau, \rho)$ have already been given in (3.5c) and (3.5d). From the boundary conditions (4.12), we find that the reduced Einstein equations (4.8) and (4.9), for the case $g = 0$, give $\mu(\tau, \rho) = 0$ and $\Phi(\tau, \rho) = 0$, so that (4.7) reproduces the flat-spacetime PDE (3.4).

C. Numerics

1. Numerical procedure

Finding the numerical solution of the PDEs (4.7), (4.8), and (4.9) is a nontrivial task. In the following local approach, we are inspired by the discussion in App. A.

The coordinates ρ and τ are put on a finite grid with N_ρ and $N_\tau = 2N_\rho$ points, respectively. The PDEs (4.7), (4.8b), and (4.8c) are then solved with time-derivatives of f and μ replaced by forward time-differences and the time-derivative of Φ replaced by a backward time-difference.

It needs to be verified that the numerically obtained functions $f(\tau, \rho)$, $\mu(\tau, \rho)$, and $\Phi(\tau, \rho)$ solve the reduced second-order Einstein equation (4.9).

2. Numerical solutions

For the presentation of our numerical results, we will employ time-slice plots (cf. Figs. 2 and 4) rather than surface plots (cf. Figs. 1 and 3). But the various time-slices will be collected in a single plot by color-coding the different time values.

The numerical solution for $g = 0$ (Fig. 5) can now be compared with the one for $g = 1/100$ (Fig. 6). For the last case, in particular, it has been verified that the numerically obtained functions $f(\tau, \rho)$, $\mu(\tau, \rho)$, and $\Phi(\tau, \rho)$ give a residual of the second-order Einstein equation (4.9) that drops to zero as the number of grid points increases.

For somewhat larger g values, a Schwarzschild-type horizon is formed, as the energy density e becomes large close to the center $\rho = 0$. This horizon is apparently different from a de-Sitter-type horizon which arises from a constant vacuum energy density far away from the center; see App. B for a brief discussion of the de-Sitter-type spacetime near the q -bubble

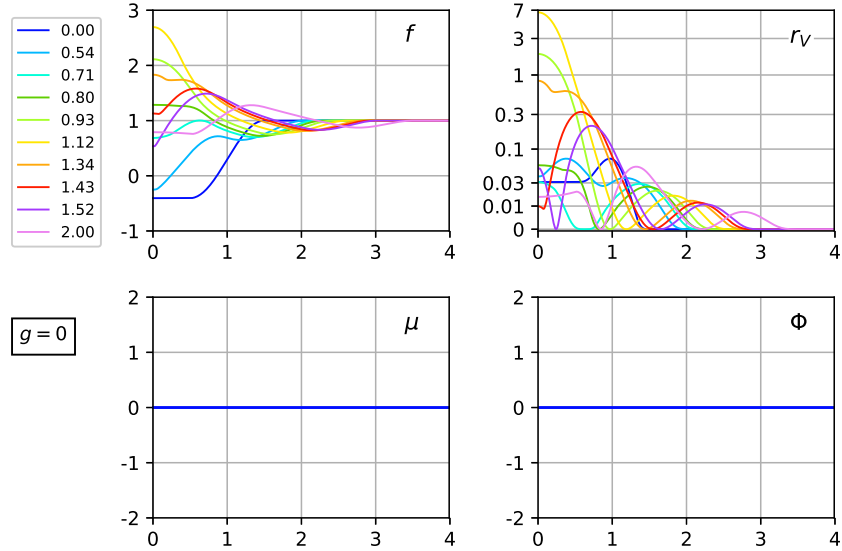


FIG. 5. Plots of $f(\tau, \rho)$, $r_V(\tau, \rho)$, $\mu(\tau, \rho)$, and $\Phi(\tau, \rho)$ at different time slices, with τ values given in the legend on the left-hand side. The model parameters are $h = 1$ and $g = 0$. The initial values are: $f(0, \rho)$ as given by (3.6) with $\bar{\rho} = 1$ and $\dot{f}(0, \rho) = 0$. The metric functions $\mu(\tau, \rho)$ and $\Phi(\tau, \rho)$ vanish identically. The vacuum energy density r_V is plotted as $\log_{10}(r_V + 0.01)$.

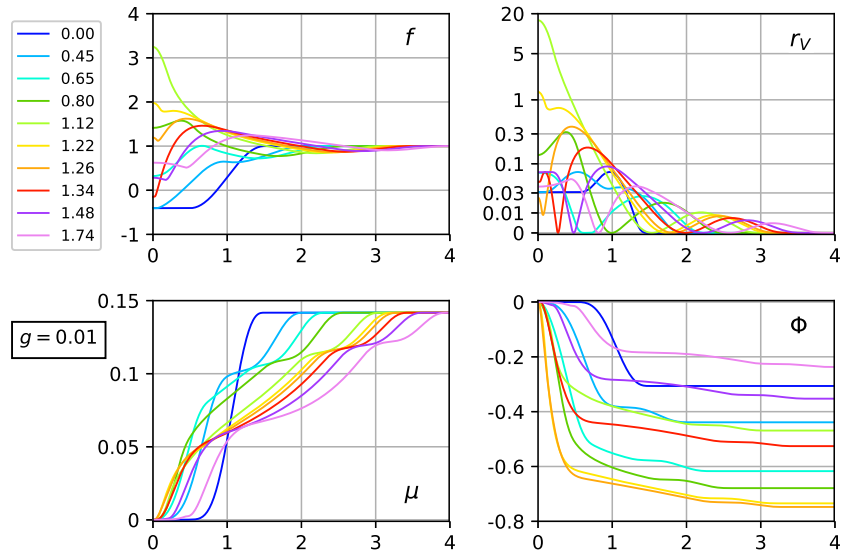


FIG. 6. Same as Fig. 5, but now for $g = 0.01$. The initial values are: $f(0, \rho)$ as given by (3.6) with $\bar{\rho} = 1$, $\dot{f}(0, \rho) = 0$, $\mu(0, \rho)$ from (4.8a), and $\Phi(0, \rho)$ from (4.8c).

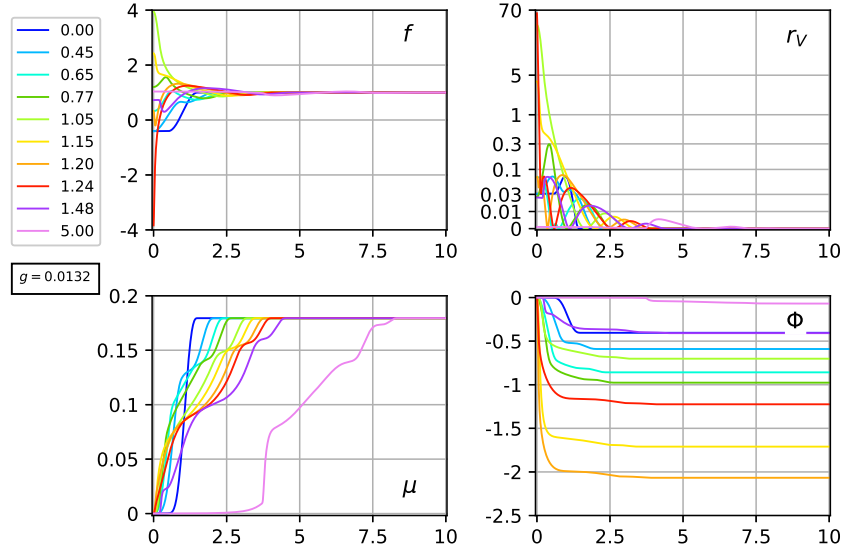


FIG. 7. Same as Fig. 6, but now for $g = 0.0132$.

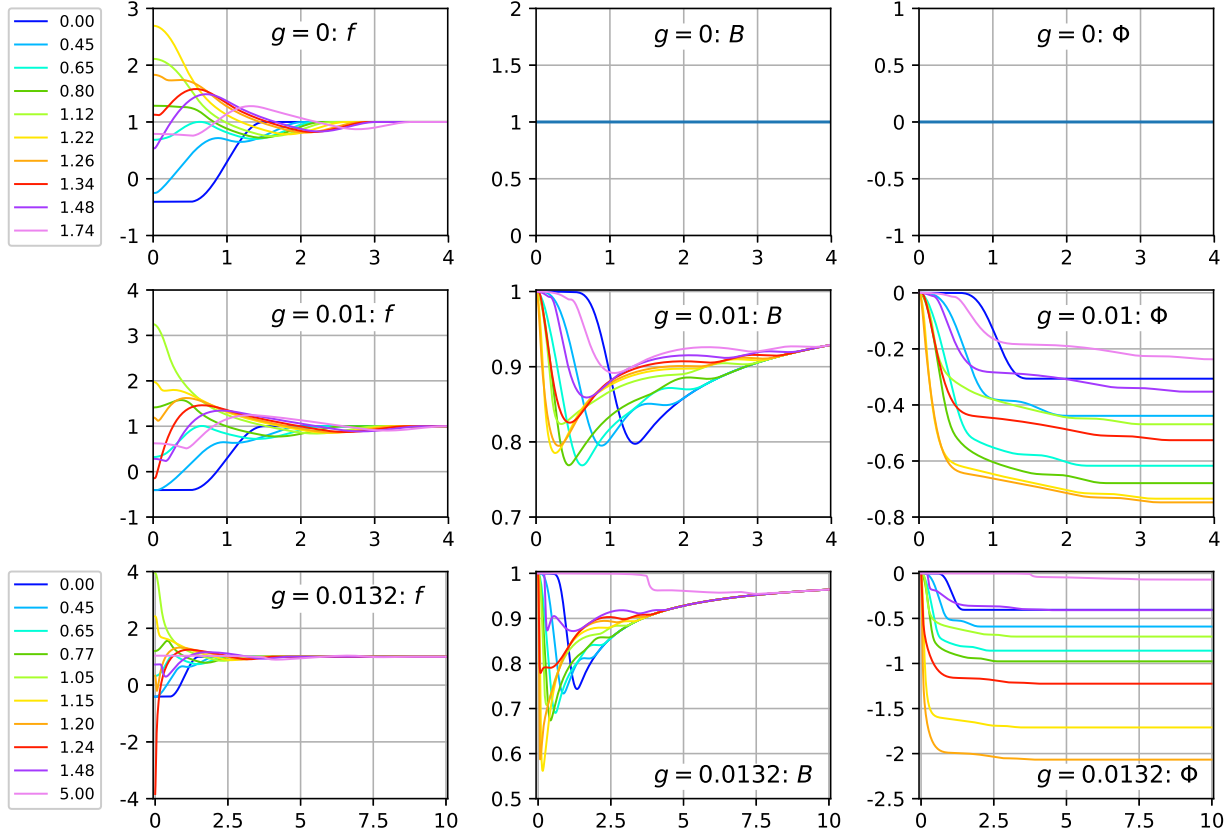


FIG. 8. Comparison of the numerical solutions at three different values of g , showing, in particular, the behavior of the quantity B from (4.6), which enters the metric (4.1). The time-slices for the top and mid rows ($g = 0$ and $g = 0.01$) are given by the upper legend on the left-hand side. The time-slices for the bottom row ($g = 0.0132$) are given by the lower legend on the left-hand side.

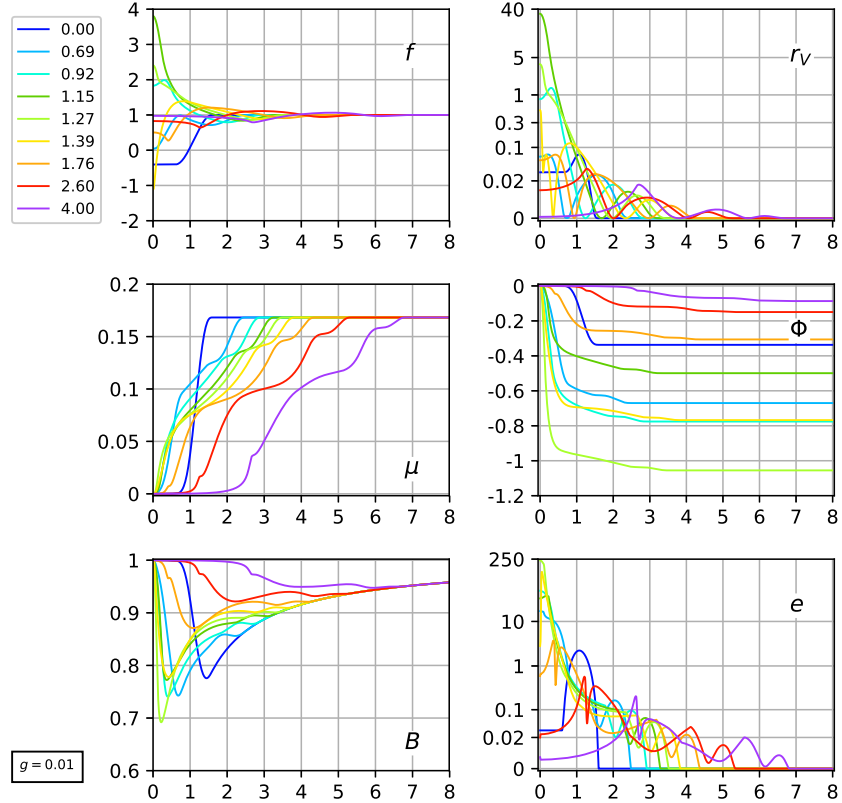


FIG. 9. Same as Fig. 6, but now with $\bar{\rho} = 1.1$ instead of $\bar{\rho} = 1$. Two additional panels show the metric quantity $B(\tau, \rho)$ from (4.6) and the energy density $e(\tau, \rho)$ from (4.11b). The energy densities e and r_V are plotted using the same scale function $\log_{10}(x + 0.005)$ but with different over-all factors. The r_V peak at $(\tau, \rho) = (1.15, 0)$ of the $\bar{\rho} = 1.1$ solution is significantly larger than the corresponding peak of the $\bar{\rho} = 1$ solution in Fig. 6. Similarly, the B dip of the $\bar{\rho} = 1.1$ solution is significantly lower than the corresponding dip of the $\bar{\rho} = 1$ solution in the B panel of the middle row of Fig. 8.

origin. With the setup and boundary conditions from Fig. 6, we estimate horizon formation to occur for $g \gtrsim 0.0133$. The regular numerical solution at $g = 0.0132$, calculated over a fine grid with $N_\tau = 100 N_\rho$, is shown in Fig. 7. The evolution towards the formation of a horizon, with $B(\tau, \rho)$ from (4.6) dipping to zero, is illustrated in Fig. 8.

For a large bubble, we expect that, from the ingoing r_V disturbance (cf. Fig. 1), the r_V peak close to the origin will be higher than the one for a small bubble. This behavior is confirmed by comparing Fig. 9 with Fig. 6. (The accuracy of the numerical solution of Fig. 9 for $\tau \gtrsim 2$ remains to be determined.) The f -panel in Fig. 9 also shows that the quantities $(\dot{f})^2$ and $(f')^2$ are large at $(\tau, \rho) \sim (1, 0)$, with both terms contributing significantly to the energy density e close to the center $\rho = 0$.

D. Discussion

The numerical results show that the vacuum energy density of a nonequilibrium q -bubble embedded in the equilibrium vacuum with $q = q_0 = \text{constant}$ evolves in a complicated way. For a sufficiently small q -bubble, part of the vacuum energy density r_V of the bubble wall, first, moves inwards towards the center and, then, rapidly disperses (cf. Fig. 1).

The numerical calculations were performed for the case with gravity turned off ($G_N = 0$) and turned on ($G_N \neq 0$). Qualitatively, the main effect of gravity is to give a larger maximum value of the vacuum energy density at the center $\rho = 0$ (compare the r_V panels of Fig. 5 and 6).

If the hierarchy ratio g from (4.4) is somewhat above 1/100, the particular solution develops a Schwarzschild-type horizon near the center $\rho = 0$ and different coordinates need to be chosen (cf. App. B). We postpone this analysis to a future publication, as the focus of the present article is on the dispersion of the vacuum energy.

V. OUTLOOK

In the present article, we have obtained a first glimpse of the inhomogeneous dynamics of the gravitating vacuum energy density $\rho_V(q)$ as described by the vacuum variable q contained in a four-form field strength. In this probe of q -theory, we start from a large vacuum energy density in a finite region of space surrounded by equilibrium vacuum, and follow the time evolution of the vacuum energy density. Our numerical results show the possibility of obtaining different evolution scenarios depending on the initial conditions and the parameters of the vacuum energy. These results suggest that there may be de-Sitter expansion within a finite region of space, gravitational collapse of the vacuum medium with the formation of a singularity, and formation of cosmological and/or black-hole horizons.

Next, we intend to study the vacuum structure of the black hole singularity. The singularity may be smoothed, as the gravitational coupling depends, in general, on the vacuum variable q and gravity may be effectively turned off near the center.

ACKNOWLEDGMENTS

The work of G.E.V. has been supported by the European Research Council (ERC) under the European Union's Horizon 2020 research and innovation programme (Grant Agreement No. 694248). O.P.S is supported by the Beca Externa Jovenes Investigadores of CONICET.

Appendix A: Integro-differential equations

The role of $\Phi(\tau, \rho)$ in the PDEs (4.7), (4.8), and (4.9) is rather subtle. From (4.8c), we have

$$\Phi' = \frac{8\pi g \rho r_V - 2\mu'/\rho}{1 - 2\mu/\rho}, \quad (\text{A1})$$

which can be integrated,

$$\widehat{\Phi}(\tau, \rho) = \int_0^\rho d\tilde{\rho} \frac{8\pi g \tilde{\rho} r_V [f(\tau, \tilde{\rho})] - 2\mu'(\tau, \tilde{\rho})/\tilde{\rho}}{1 - 2\mu(\tau, \tilde{\rho})/\tilde{\rho}}, \quad (\text{A2})$$

where the prime in the numerator of the integrand stands for differentiation with respect to $\tilde{\rho}$. Hence, $\widehat{\Phi}(\tau, \rho)$ is determined *nonlocally* by the functions $f(\tau, \tilde{\rho})$ and $\mu(\tau, \tilde{\rho})$ at the same time slice τ .

The PDEs (4.7) and (4.9) still involve Φ and its time-derivative $\dot{\Phi}$ [the spatial derivatives Φ' and Φ'' can be eliminated by use of (4.8c)]. Replacing $\Phi(\tau, \rho)$ by $\widehat{\Phi}(\tau, \rho)$ from (A2), these two equations become *integro-differential equations* solely involving the functions $f(\tau, \rho)$ and $\mu(\tau, \rho)$. Explicitly, these equations read:

$$\frac{e^{2\widehat{\Phi}}}{B} \ddot{f} - B \frac{1}{\rho^2} \partial_\rho \left(\rho^2 f' \right) + \frac{e^{2\widehat{\Phi}}}{B} \left(\partial_\tau \widehat{\Phi} + \frac{2\dot{\mu}}{\rho B} \right) \dot{f} + \left(B \widehat{\Phi}' + \frac{2\mu'}{\rho} - \frac{2\mu}{\rho^2} \right) f' = -\frac{dr_V}{df}, \quad (\text{A3a})$$

$$\frac{\mu''}{\rho} + \frac{e^{\widehat{\Phi}}}{\rho \sqrt{B}} \partial_\rho \left[\rho B^{3/2} e^{-\widehat{\Phi}} \widehat{\Phi}' \right] + \frac{e^{\widehat{\Phi}}}{\rho} \partial_\tau \left[\frac{e^{\widehat{\Phi}}}{B^2} \dot{\mu} \right] = 8\pi g \left\{ r_V + B \frac{1}{2} (f')^2 - \frac{e^{2\widehat{\Phi}}}{B} \frac{1}{2} (\dot{f})^2 \right\} \quad (\text{A3b})$$

with $\widehat{\Phi}$ given by the integral (A2) and $\partial_\tau \widehat{\Phi}$ having the τ -derivative pulled inside the integral.

Appendix B: Bubble interior

The q -bubble setup considered in this article has a start configuration $f(0, \rho)$ determined by (3.6) and the further initial condition $\dot{f}(0, \rho) = 0$. Then, the reduced field equation (4.8a) gives that the metric *Ansatz* function $\mu(\tau, \rho)$ behaves near the center as $\mu(\tau, \rho) \propto \rho^3$. This behavior of μ allows for the following definition of the quantity $h(\tau)$:

$$\lim_{\rho \rightarrow 0} \frac{2\mu(\tau, \rho)}{\rho^3} \equiv h(\tau)^2. \quad (\text{B1})$$

Near the spacetime origin ($\rho = \tau = 0$) of the q -bubble considered, we have

$$h(\tau)^2 \sim h(0)^2 \equiv h_0^2, \quad (\text{B2a})$$

$$\Phi(0, 0) \sim 0, \quad (\text{B2b})$$

$$r_V(0, 0) \sim r_{V0} > 0, \quad (\text{B2c})$$

with constants r_{V0} and h_0 . In fact, the reduced field equation (4.8a) gives

$$h_0^2 = (8\pi/3) g r_{V0}, \quad (\text{B3})$$

where g has been defined in (4.3). The resemblance of (B3) with the Friedmann equation of a universe with constant vacuum energy will become clear later on.

Writing the static metric (4.1) in terms of dimensionless variables gives

$$\begin{aligned} ds^2 = & -e^{-2\Phi(\tau, \rho)} \left[1 - \frac{2\mu(\tau, \rho)}{\rho} \right] d\tau^2 + \left[1 - \frac{2\mu(\tau, \rho)}{\rho} \right]^{-1} d\rho^2 \\ & + \rho^2 \left(d\theta^2 + \sin^2 \theta d\phi^2 \right). \end{aligned} \quad (\text{B4})$$

With the behavior (B1) and (B2), the metric (B4) near $\rho = \tau = 0$ becomes

$$ds^2 \Big|_{\text{origin}} \sim -\left[1 - h_0^2 \rho^2 \right] d\tau^2 + \left[1 - h_0^2 \rho^2 \right]^{-1} d\rho^2 + \rho^2 \left(d\theta^2 + \sin^2 \theta d\phi^2 \right), \quad (\text{B5})$$

which corresponds to the metric of de-Sitter spacetime in so-called static coordinates [21–23]. Note that, if ρ were allowed to be large enough, the metric on the right-hand side of (B5) would display a coordinate singularity at $\rho = 1/h_0$.

Now, introduce new dimensionless coordinates (denoted by a hat) from the following relations:

$$\exp(h_0 \hat{\tau}) = \sqrt{(1 - h_0^2 \rho^2)} \left[\cosh(h_0 \tau) + \sinh(h_0 \tau) \right], \quad (\text{B6a})$$

$$h_0 \hat{z} = \frac{h_0 \rho \cos \theta}{\sqrt{(1 - h_0^2 \rho^2)} \left[\cosh(h_0 \tau) + \sinh(h_0 \tau) \right]}, \quad (\text{B6b})$$

$$h_0 \hat{y} = \frac{h_0 \rho \sin \theta \cos \phi}{\sqrt{(1 - h_0^2 \rho^2)} \left[\cosh(h_0 \tau) + \sinh(h_0 \tau) \right]}, \quad (\text{B6c})$$

$$h_0 \hat{x} = \frac{h_0 \rho \sin \theta \sin \phi}{\sqrt{(1 - h_0^2 \rho^2)} \left[\cosh(h_0 \tau) + \sinh(h_0 \tau) \right]}. \quad (\text{B6d})$$

With these new coordinates, the metric (B5) near the spacetime origin of the q -bubble ($\hat{\tau} = \hat{z} = \hat{y} = \hat{x} = 0$) becomes

$$ds^2 \Big|_{\text{origin}} \sim -(d\hat{\tau})^2 + [a(\hat{\tau})]^2 \left[(d\hat{x})^2 + (d\hat{y})^2 + (d\hat{z})^2 \right], \quad (\text{B7a})$$

$$a(\hat{\tau}) \equiv \exp(h_0 \hat{\tau}). \quad (\text{B7b})$$

Note that the spatially-flat Friedmann–Robertson–Walker metric on the right-hand side of (B7a) with the scale factor (B7b) no longer has the nontrivial coordinate singularity. From the scale factor $a(\hat{\tau})$ in (B7b), we obtain $(da/d\hat{\tau})/a = h_0$, so that the quantity h_0 , which was originally defined by (B1) and (B2), can be interpreted as a Hubble constant. The scale factor $a(\hat{\tau})$ of (B7) displays, for $h_0 \hat{\tau} \gg 1$, the well-known exponential expansion of de-Sitter spacetime [21–23].

The numerical solution of Fig. 6, however, has $h_0 \approx 0.05$ for $\tau \lesssim 0.45$ and does not show the exponential expansion. Needed is an initial bubble (3.6) with $\bar{\rho} \gg 1$ (the required order of magnitude for $\bar{\rho}$ is $1/h_0 \sim 1/\sqrt{g r_V}$). But there are three problems for such large bubbles. First, as noted in Sec. III C, the numerics of a large q -bubble is challenging.

Second, the coordinate singularity of (B5) at $\rho = 1/h_0$ suggests that the metric *Ansatz* (B4) is inappropriate. Most likely, this problem can be evaded by use of another metric *Ansatz*, possibly inspired by Painlevé–Gullstrand coordinates [24–27].

Third, large bubbles may give gravitational collapse close to the center $\rho = 0$, as the energy density e from (4.11b) becomes large at the center. See Fig. 1, where the bubble-wall enhancement of the vacuum energy density r_V separates around $\tau \sim 0.4$ into an outgoing and ingoing disturbance, the latter giving a peak of r_V at $\rho = 0$ for $\tau \sim 1$. See also Fig. 9, which shows that the numerical solution with a somewhat larger value of $\bar{\rho}$ has a significantly larger r_V peak at the origin than the numerical solution of Fig. 6.

[1] Ya.B. Zel'dovich, “The cosmological constant and the theory of elementary particles,” Sov. Phys. Usp. **11**, 381 (1968).

[2] S. Weinberg, “The cosmological constant problem,” Rev. Mod. Phys. **61**, 1 (1989).

[3] M. Tanabashi *et al.* [Particle Data Group], “Review of Particle Physics,” Phys. Rev. D **98**, 030001 (2018).

[4] S.W. Hawking, “The cosmological constant is probably zero,” Phys. Lett. B **134**, 403 (1984).

[5] F.R. Klinkhamer and G.E. Volovik, “Self-tuning vacuum variable and cosmological constant,” Phys. Rev. D **77**, 085015 (2008), arXiv:0711.3170.

[6] F.R. Klinkhamer and G.E. Volovik, “Dynamic vacuum variable and equilibrium approach in cosmology,” Phys. Rev. D **78**, 063528 (2008), arXiv:0806.2805.

[7] F.R. Klinkhamer and G.E. Volovik, “Brane realization of q -theory and the cosmological constant problem,” JETP Lett. **103**, 627 (2016), arXiv:1604.06060.

[8] F.R. Klinkhamer and G.E. Volovik, “Tetrads and q -theory,” to appear in JETP Lett., arXiv:1812.07046.

[9] T. Markkanen, “De Sitter stability and coarse graining,” Eur. Phys. J. C **78**, 97 (2018), arXiv:1703.06898.

[10] H. Matsui, “Instability of de Sitter spacetime induced by quantum conformal anomaly,” JCAP **1901**, 003 (2019), arXiv:1806.10339.

[11] V.M.H. Ruutu *et al.*, “Vortex formation in neutron-irradiated superfluid ^3He as an analogue

of cosmological defect formation,” *Nature* **382**, 334 (1996).

[12] S.R. Coleman, “The fate of the false vacuum. 1. Semiclassical theory,” *Phys. Rev. D* **15**, 2929 (1977); Erratum: *Phys. Rev. D* **16**, 1248 (1977).

[13] C.G. Callan, Jr. and S.R. Coleman, “The fate of the false vacuum. 2. First quantum corrections,” *Phys. Rev. D* **16**, 1762 (1977).

[14] S.R. Coleman and F. De Luccia, “Gravitational effects on and of vacuum decay,” *Phys. Rev. D* **21**, 3305 (1980).

[15] F.R. Klinkhamer and G.E. Volovik, “Propagating q -field and q -ball solution,” *Mod. Phys. Lett. A* **32**, 1750103 (2017), arXiv:1609.03533.

[16] F.R. Klinkhamer and G.E. Volovik, “Dark matter from dark energy in q -theory,” *JETP Lett.* **105**, 74 (2017), arXiv:1612.02326.

[17] F.R. Klinkhamer and G.E. Volovik, “More on cold dark matter from q -theory,” arXiv:1612.04235v3.

[18] F.R. Klinkhamer and T. Mistelev, “Classical stability of higher-derivative q -theory in the four-form-field-strength realization,” *Int. J. Mod. Phys. A* **32**, 1750090 (2017), arXiv:1704.05436.

[19] S. Weinberg, *Gravitation and Cosmology : Principles and Applications of the General Theory of Relativity* (John Wiley and Sons, New York, 1972).

[20] G. Abreu and M. Visser, “Kodama time: Geometrically preferred foliations of spherically symmetric spacetimes,” *Phys. Rev. D* **82**, 044027 (2010), arXiv:1004.1456.

[21] E. Schrödinger, *Expanding Universes* (Cambridge University Press, Cambridge, England, 1956).

[22] S.W. Hawking and G.F.R. Ellis, *The Large Scale Structure of Space-Time* (Cambridge University Press, Cambridge, England, 1973).

[23] N.D. Birrell and P.C.W. Davies, *Quantum Fields in Curved Space* (Cambridge University Press, Cambridge, England, 1982).

[24] P. Painlevé, “La mécanique classique et la théorie de la relativité,” *C. R. Acad. Sci. (Paris)* **173**, 677 (1921).

[25] A. Gullstrand, “Allgemeine Lösung des statischen Einkörper-problems in der Einsteinschen Gravitationstheorie,” *Arkiv. Mat. Astron. Fys.* **16**, 1 (1922).

[26] K. Martel and E. Poisson, “Regular coordinate systems for Schwarzschild and other spherical space-times,” *Am. J. Phys.* **69**, 476 (2001), arXiv:gr-qc/0001069.

[27] G.E. Volovik, “Particle decay in de Sitter spacetime via quantum tunneling,” *JETP Lett.* **90**, 1 (2009), arXiv:0905.4639.